

Supplementary Information for:

**Translation factors direct intrinsic ribosome dynamics during
termination and ribosome recycling**

Samuel H. Sternberg, Jingyi Fei, Noam Prywes,
Kelly A. McGrath, and Ruben L. Gonzalez, Jr.[†]

Department of Chemistry, Columbia University, New York, NY 10027

[†]To whom correspondence should be addressed:

Ruben L. Gonzalez, Jr.

Tel: (212) 854–1096

Fax: (212) 932–1289

Email: rlg2118@columbia.edu

Keywords: Ribosome; smFRET; termination; ribosome recycling;
conformational dynamics

Running title: Translation factors direct intrinsic ribosome dynamics

SUPPLEMENTARY FIGURES

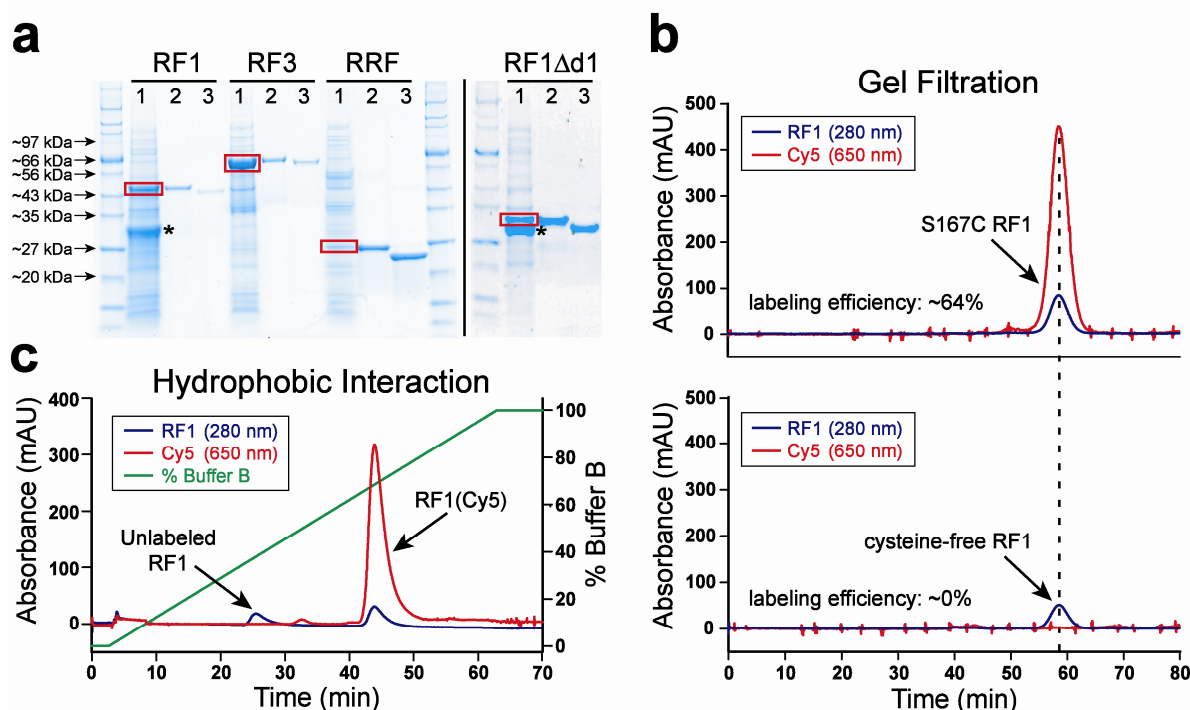


Figure 1 Purification of RFs & RRF and fluorescent labeling of RF1. **(a)** SDS-PAGE analysis of wild-type RF1, RF3, RRF, and RF1Δd1: cellular lysate after induced overexpression with 1 mM IPTG (lane 1), purified hexahistidine-tagged protein after one round of Ni²⁺-NTA chromatography (lane 2), and final protein preparations after affinity tag cleavage with TEV protease (lane 3). Overexpressed bands are boxed in red, and the asterisks in lane 1 for RF1 and RF1Δd1 denote the co-overexpressed methyltransferase (*PrmC* gene). **(b)** Gel filtration analysis of Cy5 labeling of single-cysteine S167C RF1 (top) and cysteine-free RF1 (bottom). Only RF1 with an available cysteine residue is efficiently labeled. **(c)** Separation of RF1(Cy5) from unlabeled RF1. Taking advantage of the added hydrophobicity from the Cy5 fluorophore, we purified 100% homogenously-labeled RF1(Cy5) away from unlabeled protein by injecting protein fractions from the previous gel filtration run onto a TSKgel Phenyl-5PW hydrophobic interaction column. We prepared RF1Δd1(Cy5) identically to RF1(Cy5).

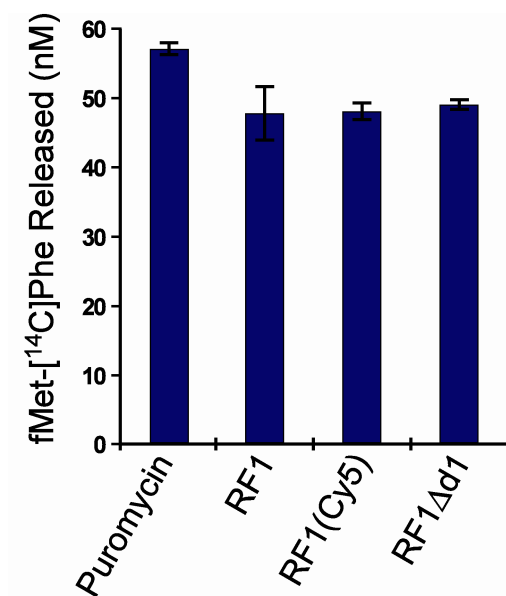


Figure 2 RF1 activity assay. We reacted release complexes (~58 nM) carrying a stop codon (UAA) at the A site and fMet-[¹⁴C]Phe-tRNA^{Phe} in the P site with puromycin (100 μM) or the RF1 construct shown (100 nM) for 1 minute at 37°C. We detected no RF1-catalyzed peptide release in identical experiments using a release complex with a sense codon (AAA) at the A site (data not shown). Error bars represent the standard deviation from three independent experiments.

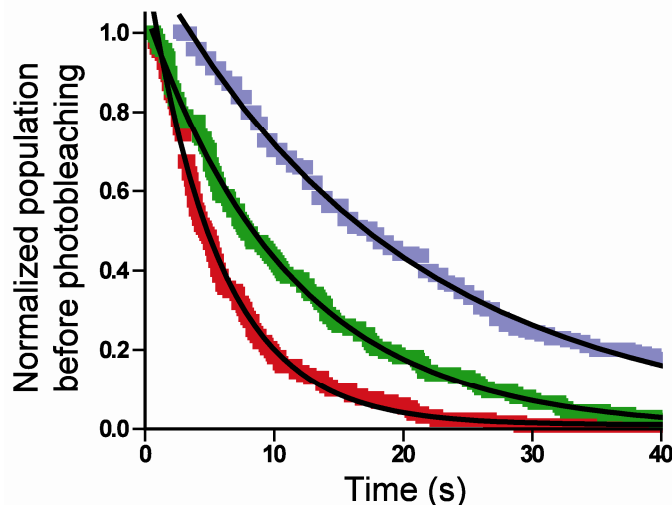


Figure 3 Analysis of photobleaching rate for smFRET_{RF1-tRNA} signal. We recorded data using 532 nm laser excitation powers of 24 mW (red), 12 mW (green), or 24 mW chopped laser pulses which illuminated the sample for 50 ms every 250 ms (blue). After manually determining the length of every smFRET trajectory before photobleaching of either Cy3 or Cy5, we plotted one-dimensional histograms of trajectory length. Because we required all analyzed smFRET trajectories to last longer than 10 frames, we removed the first 10 frames of data from the histograms before fitting the data to single exponential decays (black lines) of the form $A \times \exp-(x-x_0/\tau)+y_0$, with x_0 manually set to 0.55 seconds (24 mW and 12 mW) or 2.68 seconds (24 mW with laser chopping). We obtained the following parameters: $y_0 = 0.0097$, $A = 1.061$, $\tau = 5.51 \pm 0.02$ s (24 mW, red); $y_0 = -0.001$, $A = 1.005$, $\tau = 11.22 \pm 0.05$ s (12 mW, green); and $y_0 = 0.0063$, $A = 1.032$, $\tau = 19.46 \pm 0.07$ s (24 mW with laser chopping, blue). Taking the inverse of each lifetime yielded the following rates for the loss of fluorescence signal: 0.1814 ± 0.0008 s⁻¹, 0.0892 ± 0.0004 s⁻¹, and 0.0514 ± 0.0002 s⁻¹, respectively. The R² of all fits was greater than 0.99. The clear dependence of the rate of loss of the fluorescence signal on laser excitation power and excitation time demonstrates that loss of fluorescence is due to photobleaching rather than dissociation of RF1(Cy5) from RC1.

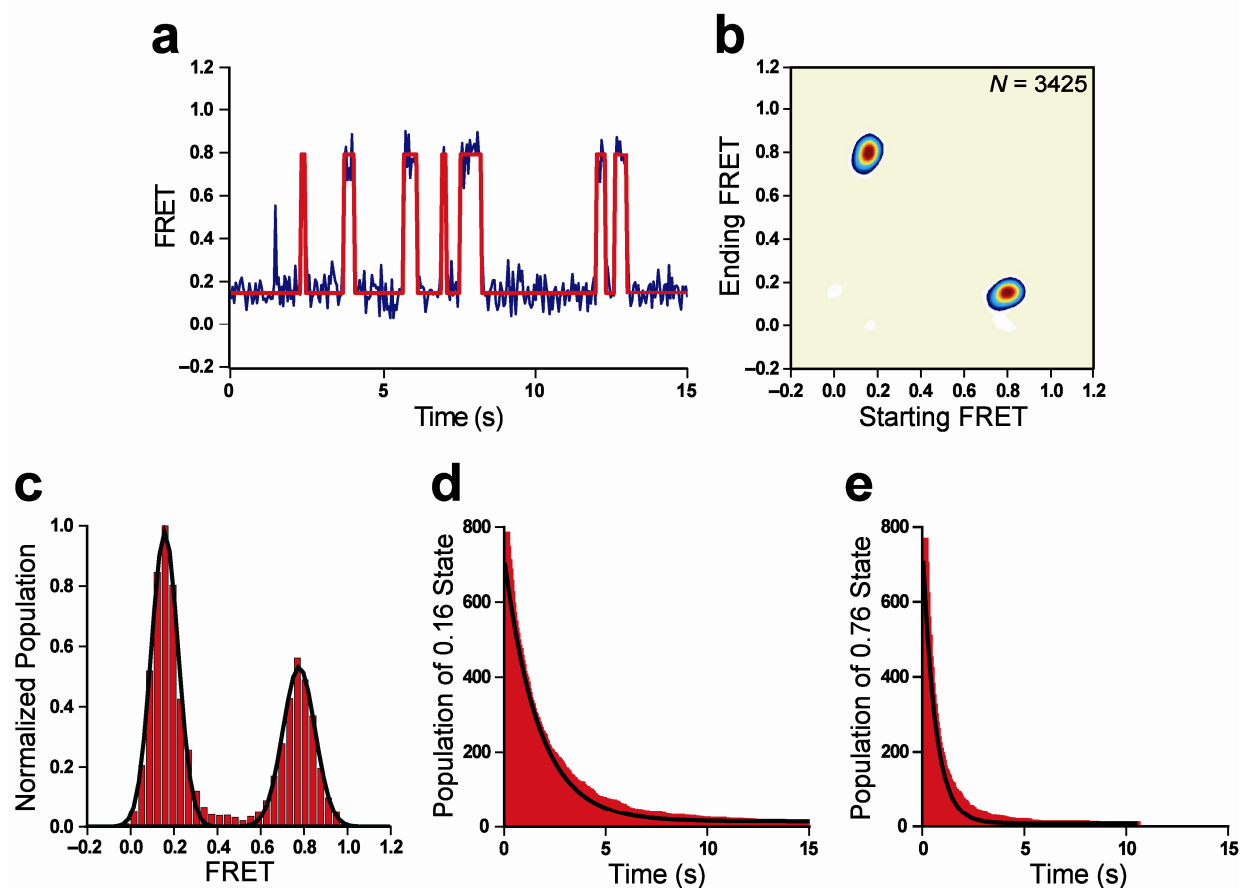


Figure 4 Representative kinetic analysis of RC2_{Pmn}. **(a)** Using the HaMMY software suite¹, we converted raw smFRET data (blue) into idealized smFRET data (red) with hidden Markov modeling. A representative smFRET trajectory is shown. **(b)** We generated a transition density plot by plotting the “Starting FRET” vs. “Ending FRET” for each transition in a given dataset as contour plots of two-dimensional population histograms. Contours are shown from tan (lowest population) to red (highest population), with “*N*” indicating the number of transitions. **(c)** We generated one-dimensional smFRET histograms (red bars) from the first 0.5 seconds of all traces, and defined thresholds for the 0.16 (0.10–0.22) and 0.76 (0.70–0.85) FRET states by the full width at half height of each Gaussian fit (black line). **(d,e)** Population histograms of dwell time spent in the 0.16 **(d)** and 0.76 **(e)** FRET states (red bars) are well described by single exponential decays (black lines) of the form $A \times \exp(-(x/\tau) + y_0)$. We obtained the

Sternberg *et al.*

following parameters from these two representative fits: $y_0 = 4.5$, $A = 703$, $\tau = 1.79 \pm 0.01$ s (0.16 FRET state) and $y_0 = 8.0$, $A = 755$, $\tau = 0.615 \pm 0.009$ s (0.76 FRET state), yielding $k_{GS1 \rightarrow GS2} = 0.492 \pm 0.003$ s⁻¹ and $k_{GS2 \rightarrow GS1} = 1.32 \pm 0.02$ s⁻¹ after correcting for photobleaching rates and the length of observation time. The R^2 of both fits was greater than 0.99. The final values of $k_{GS1 \rightarrow GS2} = 0.52 \pm 0.03$ s⁻¹ and $k_{GS2 \rightarrow GS1} = 1.36 \pm 0.03$ s⁻¹ reported in the text of the manuscript are the averages and standard deviations of three independently recorded and equivalently analyzed datasets.

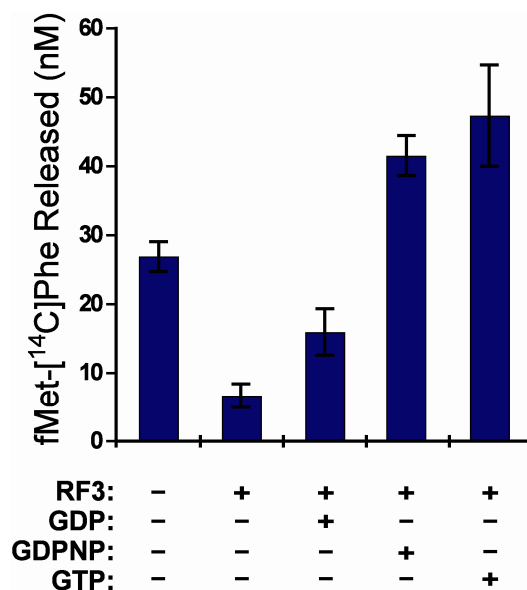


Figure 5 RF3 activity assay. We reacted release complexes (~58 nM) carrying a stop codon (UAA) at the A site and fMet-[¹⁴C]Phe-tRNA^{Phe} in the P site with substoichiometric wild-type RF1 (5 nM) and, when present, RF3 (200 nM) and the nucleotide shown (0.2 mM) for 10 minutes at 37°C. The nucleotide dependency of RF3-catalyzed RF1 recycling agrees with that demonstrated previously². Error bars represent the standard deviation from three independent experiments.

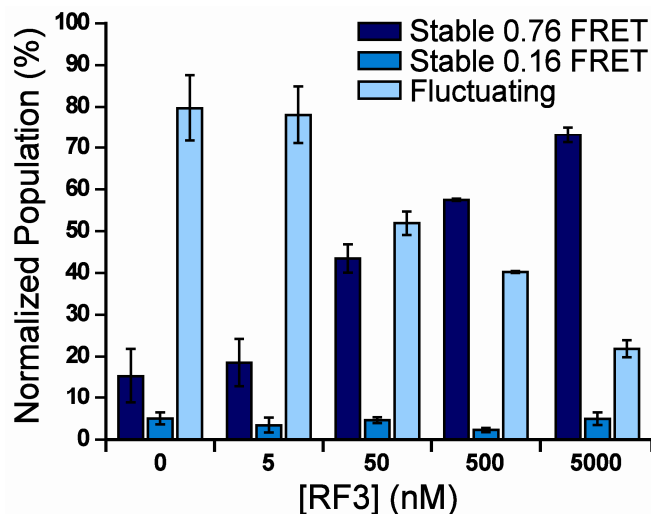


Figure 6 Subpopulation analysis of RC2_{P_{mn}} + RF3(GDPNP) titration. We collected data from RC2_{P_{mn}} alone or RC2_{P_{mn}} in the presence of 1 mM GDPNP and the concentration of RF3 shown, and grouped resulting smFRET trajectories into one of three subpopulations: stable 0.76 FRET (GS2; dark blue), stable 0.16 FRET (GS1; medium blue), or fluctuating trajectories showing transitions between 0.76 and 0.16 FRET (light blue). As RF3 concentration increases, the relative occupancy of the fluctuating subpopulation decreases as progressively more trajectories exhibit stable 0.76 FRET, corresponding to RF3(GDPNP)-bound RCs. Error bars represent the standard deviation from multiple datasets (0 nM RF3) or after splitting each dataset into three equal parts and analyzing subpopulations for each part separately.

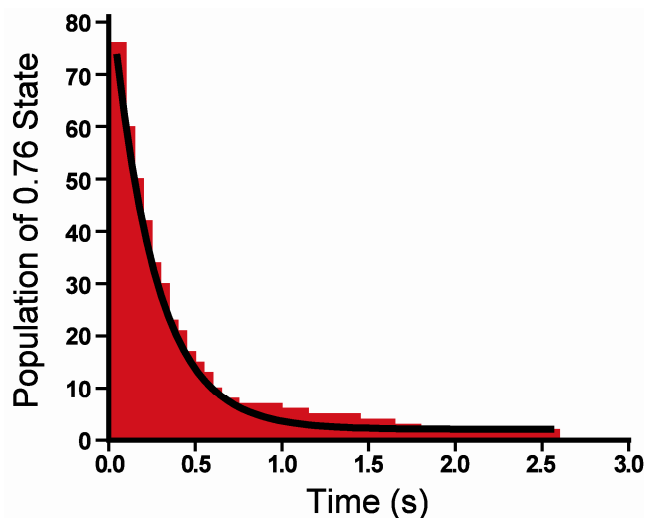


Figure 7 Kinetic analysis of $k_{GS2 \rightarrow GS1}$ for $RC2_{RF1} + RF3(GDP) + GTP$. We split the dataset into three equal parts, and independently fit one-dimensional histograms of time spent in GS2 for each third of the dataset with a single-exponential decay (black line) of the form $A \times \exp(-(x/\tau) + y_0)$. We obtained the following parameters from a representative third: $y_0 = 2.1$, $A = 87$, $\tau = 0.249 \pm 0.005$ s ($R^2 = 0.99$), yielding $k_{GS2 \rightarrow GS1} = 3.71 \pm 0.08$ s $^{-1}$ after correcting for photobleaching rate and the length of observation time. The final value of $k_{GS2 \rightarrow GS1} = 3.7 \pm 0.6$ s $^{-1}$ reported in the text of the manuscript is the average and standard deviation of independent fitting and analysis of each third of the dataset.

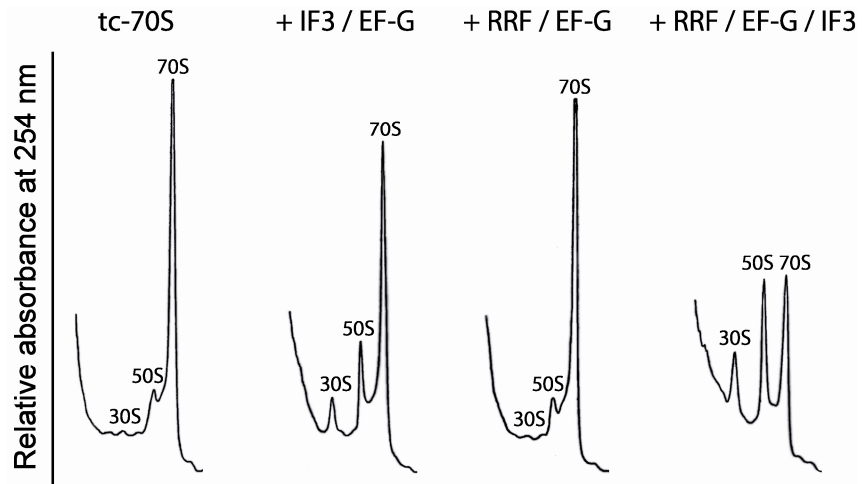


Figure 8 RRF activity assay. We incubated tightly-coupled 70S ribosomes ($0.2 \mu\text{M}$) alone or with 0.5 mM GTP and the proteins shown ($[\text{IF3}] = 5 \mu\text{M}$, $[\text{EF-G}] = 20 \mu\text{M}$, $[\text{RRF}] = 20 \mu\text{M}$) for 20 minutes at 37°C in Tris-polymix buffer, 6 mM $\text{Mg}(\text{OAc})_2$. We loaded reactions onto sucrose gradients and analyzed them as described in the Supplementary Methods. Sedimentation is from left to right, and peaks for 30S, 50S, and 70S ribosomes are indicated. We carried out each experiment at least twice; data from representative sucrose gradients are shown.

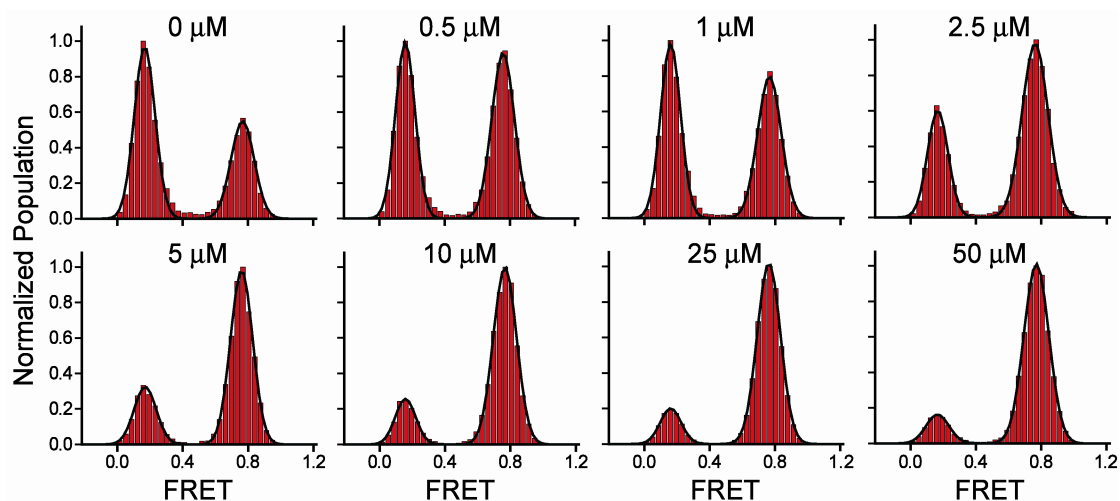


Figure 9 One-dimensional smFRET histograms of RC2_{Pmn} + RRF titration. We collected data from RC2_{Pmn} alone or RC2_{Pmn} in the presence of the concentration of RRF shown, and generated one-dimensional histograms (red bars) using the first 10 frames of resulting smFRET data. Fits of the two Gaussian distributions in each histogram (black lines) yield population information for GS1 (0.16 FRET) and GS2 (0.76 FRET), and the GS2/GS1 peak area ratio defines the equilibrium constant (K_{eq}) governing the GS1 \rightleftharpoons GS2 equilibrium at every RRF concentration.

SUPPLEMENTARY METHODS

Cloning of RF1, RF1 Δ d1, RF3, RRF, and methyltransferase. We cloned genes encoding RF1, RF3, and RRF from *Escherichia coli* C600 genomic DNA into the pProEx-HTb vector (Invitrogen) using KsaI (5') and KpnI (3') restriction sites, which places the gene under Trc promoter control and appends an N-terminal hexahistidine affinity tag and downstream TEV protease cleavage site. Enzymatic cleavage of the affinity tag leaves an extraneous GA dipeptide at the N terminus of each protein factor. We cloned the *PrmC* gene encoding the RF1-modifying methyltransferase into the pET-26b(+) vector (Novagen) using NdeI (5') and HindIII (3') restriction sites; we avoided appendage of the optional C-terminal hexahistidine affinity tag by placing a stop codon at the C terminus of the gene. We generated the RF1 Δ d1 construct by deleting the region of the *PrfA* gene encoding amino acids 1–89, as previously described³. To enable site-specific Cy5-labeling of RF1 and RF1 Δ d1, we generated a single-cysteine mutant previously shown to retain wild-type activity⁴ by mutating all wild-type cysteines to serines (C51S C201S C257S) and engineering an additional S167C mutation into RF1 domain 2 using the Quikchange Mutagenesis Kit (Stratagene). We verified all clones by DNA sequencing.

Preparation of IFs, EFs, tRNAs, mRNA and L1(Cy5) ribosomes. We purified initiation and elongation factors as previously described⁵. We labeled tRNA^{Phe} (Sigma-Aldrich) with Cy3-NHS ester (GE Healthcare) at the naturally occurring acp³U modification at position 47, and purified it using hydrophobic interaction chromatography⁵. We aminoacylated tRNA^{fMet} (MP Biomedicals), tRNA^{Phe}, and (Cy3)tRNA^{Phe}, and formylated Met-tRNA^{fMet}, following previously published protocols⁵. The mRNA used in these studies is derived from the mRNA encoding gene product 32 from T4 bacteriophage. The sequence of this mRNA is: **GGCAACCUAAAACUACACAGGGCCCUAAGGAAAUAAAAUGUUUUAAUGUAAA** UCUACUGCUGAACUCGCUGCACAAAUGGCUAAACUGAAUGGCAAUUAAGGAUC, where the nucleotides in bold are a 26 nucleotide spacer region containing an 18 nucleotide sequence (underlined in bold) to which we hybridized a complementary 3'-

biotinylated DNA oligonucleotide (IDT; TGTGTAAGTTTTAGGTTGATTTG-Biotin) to enable surface immobilization. This was followed by a strong Shine-Dalgarno ribosomal binding site (underlined), an open reading frame encoding fMet-Phe-STOP within a strong stop codon context⁶ (underlined in italics), and 58 additional downstream nucleotides. For control experiments with a sense codon, the mRNA was identical except for the beginning of the open reading frame sequence, which we mutated to AUG UUU AAA C. We constructed L1(Cy5) ribosomes as previously described⁷.

Fluorescent labeling of RF1 and RF1 Δ d1. We reacted single-cysteine S167C RF1 and RF1 Δ d1 mutants with a ~20-fold molar excess of Cy5-maleimide (GE Healthcare) overnight at 4°C in Protein Labeling Buffer (100 mM Tris-OAc, pH_{25°C} = 7.0, 50 mM KCl, 1 mM tris(2-carboxyethyl)phosphine hydrochloride). We subsequently injected the reaction onto a 60 cm HiLoad Superdex 75 gel filtration column (GE Healthcare) pre-equilibrated against Gel Filtration Buffer (20 mM Tris-Cl, pH_{4°C} = 7.5, 100 mM KCl, 10 mM 2-mercaptoethanol), and separated RF1/RF1 Δ d1 from unreacted dye by elution with 1.5 column volumes of Gel Filtration Buffer running at a flow rate of 1 ml min⁻¹ (Supplementary Fig. 1b). RF1, RF1 Δ d1, and unreacted dye eluted at 59, 65, and 113 minutes, respectively. We concentrated and exchanged protein fractions into Buffer A (100 mM Na₂HPO₄, pH_{25°C} = 7.0, 1 M (NH₄)₂SO₄), and subsequently injected the sample onto a TSKgel Phenyl-5PW hydrophobic interaction column (Tosoh Bioscience) pre-equilibrated against Buffer A. We separated Cy5-labeled RF1/RF1 Δ d1 from unlabeled RF1/RF1 Δ d1 by elution with a Buffer B (100 mM Na₂HPO₄, pH_{25°C} = 7.0) gradient extending from 0% to 100% over 60 minutes running at a flow rate of 1 ml min⁻¹ (Supplementary Fig. 1c). RF1, RF1 Δ d1, RF1(Cy5), and RF1 Δ d1(Cy5) eluted at 38%, 35%, 68%, and 70% Buffer B, respectively. This purification procedure yields 100% homogenously-labeled RF1(Cy5)/RF1 Δ d1(Cy5).

RF1 and RF3 activity assays. We formed radioactive release complexes following a similar protocol as with RC1 but using [¹⁴C]Phe-tRNA^{Phe} during the elongation step rather than Phe-(Cy3)tRNA^{Phe}. Additionally, instead of sucrose density gradient

ultracentrifugation, we separated release complexes from free GTP and GDP by buffer exchange into fresh Tris-polymix buffer, 5 mM Mg(OAc)₂, using two successive Micro Bio-Spin 30 chromatography columns (Bio-Rad Laboratories). We then aliquoted and froze release complexes in liquid nitrogen, and stored at -80°C . Release complexes were $\sim 85\%$ active in peptide bond formation, as determined by the efficiency of deacylating P-site fMet-[¹⁴C]Phe-tRNA^{Phe} with the antibiotic puromycin.

We tested wild-type RF1, RF1(Cy5), RF1 Δ d1, and RF1 Δ d1(Cy5) for peptide release activity following previously published protocols⁸, and estimated the proportion of active RF1 for each individual construct by single-round dipeptide release in the presence of excess RF3 without guanine nucleotide². Briefly, we pre-incubated release complexes and RF1 (with RF3) separately for 1 minute at 37°C , and then mixed and reacted them at 37°C for 1 minute. We quenched reactions by adding an equal volume of ice-cold 25% formic acid, and after a 15 minute incubation on ice, we separated precipitated components from any released dipeptide by microcentrifugation at $14,000\times g$. We determined the extent of peptide hydrolysis by measuring the radioactivity in both the pellet and supernatant with scintillation counting, subtracting the amount of background peptide release from a buffer reaction control, and using a calibration curve to deduce the molar amount of dipeptide released based on the counts per minute (cpm). Percent activities, calculated as the amount of dipeptide released divided by the amount of RF1 in the reaction, were 30–40% for wild-type RF1 and RF1(Cy5), and $\sim 10\%$ for RF1 Δ d1 and RF1 Δ d1(Cy5), in general agreement with published literature values². We tested the stop-codon dependence of RF1-catalyzed peptide release by reacting RF1 with release complexes stalled on a lysine codon (AAA) at position three instead of a stop codon (UAA); we detected no dipeptide release above background for any of the RF1 constructs. RF1 concentrations given in captions for Supplementary Figures 2 and 5 correspond to active concentrations.

We tested RF3 activity by following the extent of peptide release in cases where RF1 was limiting and RF3 was required to actively recycle RF1, thereby enabling multiple turnover². We carried out reactions identically as above, with two exceptions: when present, we added GDP, GTP, or GDPNP to the RF1/RF3 mix during the 1 minute pre-incubation, and upon adding the RF1/RF3/nucleotide mix to release

complexes, we incubated reactions for 10 minutes. Supplementary Figure 5 demonstrates that RF3 exhibits the proper nucleotide dependence in recycling RF1.

RRF activity assay. We tested RRF for its ability to split 70S ribosomes into 30S and 50S subunits, as detected by sucrose density gradient ultracentrifugation, following a previously published protocol⁹. Briefly, reaction mixtures consisting of 0.2 μ M tightly-coupled 70S ribosomes and a combination of 20 μ M RRF, 20 μ M EF-G, 5 μ M IF3 and 0.5 mM GTP, were reacted for 20 minutes at 37°C in Tris-polymix buffer, 6 mM Mg(OAc)₂. After a brief incubation on ice, we subsequently loaded reaction mixtures onto a 10%–40% sucrose density gradient in the same Tris-polymix buffer, followed by ultracentrifugation in an SW40 rotor (Beckman Coulter) at 25,000 rpm for 12 hours at 4°C. We analyzed gradients by monitoring the absorbance at 254 nm with a gradient analyzer (Brandel); the extent of 70S dissociation under our conditions is in agreement with previously published results⁹ (Supplementary Fig. 8).

Selection of single-molecule FRET trajectories. We analyzed raw intensity data with the Metamorph software suite (Molecular Devices). For RF1-tRNA smFRET experiments with RC1, we selected molecules for further analysis that exhibited Cy5 fluorescence *via* FRET above a minimum threshold of 1000 Arbitrary Units in frame one of each steady-state movie, denoting an RF1-bound release complex. For L1-tRNA smFRET experiments with RC2, we directly excited Cy5 with the 643 nm laser in frame one, followed by excitation with the 532 nm laser in order to generate FRET; we selected all molecules that exhibited Cy5 fluorescence *via* direct excitation in frame one for further analysis. We then visually inspected acquired trajectories, composed of a pair of Cy3 and Cy5 intensity *versus* time trajectories from single ribosomes, and kept trajectories exhibiting characteristic single-fluorophore fluorescence intensities and single-step fluorophore photobleaching for further analysis. For all RRF and RF3(GDPNP) datasets, we first utilized an automated selection algorithm before visual inspection of the trajectories, which averages each trajectory over three data points, differentiates intensity with respect to time, and calculates the correlation coefficient for each Cy3/Cy5 pair. Trajectories with a negative correlation coefficient (anti-correlated)

were kept for further analysis. Finally, we required all trajectories to last at least 0.5 seconds (i.e. 10 frames) before photobleaching of either fluorophore.

We baseline-corrected Cy3 and Cy5 fluorescence intensities in each trajectory by generating one-dimensional Cy3 and Cy5 fluorescence intensity histograms from trajectories within each dataset, determining the intensity value of the most populated bin (which represents background noise intensity after fluorophore photobleaching), and then subtracting this value from all Cy3 and Cy5 intensity data points within every trajectory. Finally, due to the imperfect performance of emission filters, we experimentally determined the Cy3 signal bleed-through into the Cy5 channel to be ~9% in our experimental system. We therefore corrected the Cy5 intensity of each trajectory using this bleed-through coefficient. We calculated smFRET values for each Cy3/Cy5 data point using $I_{\text{Cy5}}/(I_{\text{Cy3}}+I_{\text{Cy5}})$, where I_{Cy3} and I_{Cy5} are the intensities of Cy3 and Cy5, respectively.

Corrections to $k_{\text{GS1} \rightarrow \text{GS2}}$ and $k_{\text{GS2} \rightarrow \text{GS1}}$. Because all fluctuating smFRET trajectories for our L1 stalk-tRNA FRET signal were prematurely truncated by either Cy3 or Cy5 photobleaching or, more rarely, by the length of our observation time (60 seconds), measured rates for $\text{GS1} \rightarrow \text{GS2}$ ($k_{\text{GS1} \rightarrow \text{GS2}}$) and $\text{GS2} \rightarrow \text{GS1}$ ($k_{\text{GS2} \rightarrow \text{GS1}}$) transitions will be systematically overestimated¹⁰. Therefore, to account for the rates of photobleaching and the limited observation time, we applied a uniform correction to all observed values for $k_{\text{GS1} \rightarrow \text{GS2,obs}}$ and $k_{\text{GS2} \rightarrow \text{GS1,obs}}$ using the following equations¹⁰:

$$k_{\text{GS1} \rightarrow \text{GS2}} = k_{\text{GS1} \rightarrow \text{GS2,obs}} - k_{\text{photobleach,GS1}} - 1/T$$

$$k_{\text{GS2} \rightarrow \text{GS1}} = k_{\text{GS2} \rightarrow \text{GS1,obs}} - k_{\text{photobleach,GS2}} - 1/T$$

where $k_{\text{photobleach,GS1}}$ and $k_{\text{photobleach,GS2}}$ are the photobleaching rates from the FRET states corresponding to GS1 and GS2, respectively, and T is the observation time (60 seconds). We measured $k_{\text{photobleach,GS1}}$ by averaging the rate of photobleaching for stable 0.16 smFRET trajectories from the following datasets: $\text{RC2}_{\text{Pmn}} + \text{RF1}$, RC2_{RF1} , $\text{RC2}_{\text{RF1}} + \text{RF3}$ (nucleotide free), and $\text{RC2}_{\text{RF1}} + \text{RF3}$ (GDP). We measured $k_{\text{photobleach,GS2}}$ by averaging the rate of photobleaching for stable 0.76 FRET trajectories from the following datasets: $\text{RC2}_{\text{Pmn}} + 50 \mu\text{M RRF}$, $\text{RC2}_{\text{Pmn}} + 1 \mu\text{M RF3}$ (GDPNP), and $\text{RC2}_{\text{Pmn}} +$

Sternberg *et al.*

5 μM RF3(GDPNP). We determined $k_{\text{photobleach,GS1}}$ and $k_{\text{photobleach,GS2}}$ to be $0.05 \pm 0.01 \text{ s}^{-1}$ and $0.29 \pm 0.03 \text{ s}^{-1}$, respectively. All values for $k_{\text{GS1} \rightarrow \text{GS2}}$ and $k_{\text{GS2} \rightarrow \text{GS1}}$ given in the text and figures correspond to corrected rates.

REFERENCES

1. McKinney, S.A., Joo, C. & Ha, T. Analysis of single-molecule FRET trajectories using hidden Markov modeling. *Biophys J* **91**, 1941-1951 (2006).
2. Zavialov, A.V., Buckingham, R.H. & Ehrenberg, M. A posttermination ribosomal complex is the guanine nucleotide exchange factor for peptide release factor RF3. *Cell* **107**, 115-124 (2001).
3. Mora, L., Zavialov, A., Ehrenberg, M. & Buckingham, R.H. Stop codon recognition and interactions with peptide release factor RF3 of truncated and chimeric RF1 and RF2 from *Escherichia coli*. *Mol Microbiol* **50**, 1467-1476 (2003).
4. Wilson, K.S., Ito, K., Noller, H.F. & Nakamura, Y. Functional sites of interaction between release factor RF1 and the ribosome. *Nat Struct Biol* **7**, 866-870 (2000).
5. Blanchard, S.C., Kim, H.D., Gonzalez, R.L., Jr., Puglisi, J.D. & Chu, S. tRNA dynamics on the ribosome during translation. *Proc Natl Acad Sci U S A* **101**, 12893-12898 (2004).
6. Pavlov, M.Y. *et al.* A direct estimation of the context effect on the efficiency of termination. *J Mol Biol* **284**, 579-590 (1998).
7. Fei, J., Kosuri, P., MacDougall, D.D. & Gonzalez, R.L., Jr. Coupling of ribosomal L1 stalk and tRNA dynamics during translation elongation. *Mol Cell* **30**, 348-359 (2008).
8. Freistroffer, D.V., Pavlov, M.Y., MacDougall, J., Buckingham, R.H. & Ehrenberg, M. Release factor RF3 in *E. coli* accelerates the dissociation of release factors RF1 and RF2 from the ribosome in a GTP-dependent manner. *EMBO J* **16**, 4126-4133 (1997).
9. Hirokawa, G. *et al.* The role of ribosome recycling factor in dissociation of 70S ribosomes into subunits. *RNA* **11**, 1317-1328 (2005).
10. Bartley, L.E., Zhuang, X., Das, R., Chu, S. & Herschlag, D. Exploration of the transition state for tertiary structure formation between an RNA helix and a large structured RNA. *J Mol Biol* **328**, 1011-1026 (2003).